




# Article

# The Valorisation of Selected Quarry and Mine Waste for Sustainable Cement Production within the Concept of Circular Economy

Emilija Fidanchevski <sup>1</sup>, Katarina Šter <sup>2</sup>, Maruša Mrak <sup>2</sup>, Ljiljana Kljajević <sup>3</sup>, Gorazd Žibret <sup>4</sup>, Klemen Teran <sup>4</sup>, Bojan Poletanovic <sup>5</sup>, Monika Fidanchevska <sup>1</sup>, Sabina Dolenc <sup>2</sup> and Ildiko Merta <sup>5,\*</sup>

- <sup>1</sup> Faculty of Technology and Metallurgy, Ss. Cyril and Methodius University in Skopje, Rugjer Boshkovich 16, 1000 Skopje, North Macedonia; emilijaf@tmf.ukim.edu.mk (E.F.); fidancevskam97@gmail.com (M.F.)
  - <sup>2</sup> Slovenian National Building and Civil Engineering Institute, Dimičeva ulica 12, 1000 Ljubljana, Slovenia; katarina.ster@zag.si (K.Š.); marusa.mrak@zag.si (M.M.); sabina.dolenc@zag.si (S.D.)
  - <sup>3</sup> Department of Materials, „VINČA” Institute of Nuclear Sciences—National Institute of the Republic of Serbia, University of Belgrade, Mike Petrovića Alasa 12–14, 11000 Belgrade, Serbia; ljiljana@vinca.rs
  - <sup>4</sup> Geological Survey of Slovenia, 1000 Ljubljana, Slovenia; gorazd.zibret@geo-zs.si (G.Ž.); klemen.teran@geo-zs.si (K.T.)
  - <sup>5</sup> TU Wien Faculty of Civil Engineering, Institute of Material Technology, Building Physics and Building Ecology, Karlsplatz 13/E207-2, 1040 Vienna, Austria; bojan.poletanovic@tuwien.ac.at
- \* Correspondence: ildiko.merta@tuwien.ac.at



**Citation:** Fidanchevski, E.; Šter, K.; Mrak, M.; Kljajević, L.; Žibret, G.; Teran, K.; Poletanovic, B.; Fidanchevska, M.; Dolenc, S.; Merta, I. The Valorisation of Selected Quarry and Mine Waste for Sustainable Cement Production within the Concept of Circular Economy. *Sustainability* **2022**, *14*, 6833. <https://doi.org/10.3390/su14116833>

Academic Editor: Chongchong Qi

Received: 31 March 2022

Accepted: 27 May 2022

Published: 2 June 2022

**Publisher’s Note:** MDPI stays neutral with regard to jurisdictional claims in published maps and institutional affiliations.



**Copyright:** © 2022 by the authors. Licensee MDPI, Basel, Switzerland. This article is an open access article distributed under the terms and conditions of the Creative Commons Attribution (CC BY) license (<https://creativecommons.org/licenses/by/4.0/>).

**Abstract:** The cement industry could potentially consume large amounts of solid industrial waste in order to improve its sustainability. The suitability of selected quarry and mine waste as secondary raw materials (SRM) was examined for the sustainable production of cement following the concept of a circular economy. The chemical, mineralogical, and radiological characterization of SRM was conducted in this study. Its potential use in low-carbon and low-energy belite-sulfoaluminate cement was investigated by incorporating the examined SRM into cement clinker. Various characterization methods were used to characterize the cement, including X-ray powder diffraction (XRD), thermal analysis (DTA/TG), and isothermal calorimetry. Depending on the chemical composition of the waste, lower or higher amounts were allowed to be incorporated into the raw clinker mixture for a targeted clinker phase composition. Among the samples, differences were observed in the phase composition of synthesized clinkers, which slightly influenced the reactivity of the cement but did not significantly change the compressive strength of the final product.

**Keywords:** BCSA clinker; cement; circular economy; clinker; mine wastes; quarry waste

## 1. Introduction

The construction industry is one of the greatest emitters of CO<sub>2</sub> and the production of cement, which is the most widely used construction material on Earth, but also one of the most responsible for the global anthropogenic greenhouse gas emissions [1]. The main reason for the high emission rate is the extremely energy-demanding nature of producing Portland cement clinker. Namely, the production process requires approximately 850 kcal and is responsible for up to 1 kg of CO<sub>2</sub>/kg of cement produced [2]. About 60% of this is emitted through the calcination process of limestone, while the rest results from the combustion of fuel in the clinker kiln. Since the cement consumption has exploded in the last two decades (from 1.6 to 4.4 billion metric tons), the current situation with the use of cement in terms of the ecology is alarming [3]. Additionally, a further increase in cement consumption in the future is predicted [4]. In recent years the cement industry has been investing significant efforts in decreasing the environmental impact of OPC production by examining different approaches, including (i) employing sustainable combustion methods, (ii) lowering the energy needed for cement production, (iii) decreasing the percentage

of clinker in cement, (iv) investigating carbon capture and storage, and (v) the use of alternative low CO<sub>2</sub> binders or non-OPC binders [5,6]. The final option is one of the most promising approaches since it is based on the valorization of various wastes, residues, and industrial by-products, including coal fly ash and bottom ash, slag from the iron and steel industry, red mud, mine, and quarry waste, and paper sludge, among others [7]. Recently, growing environmental awareness and the necessity to reduce both the consumption of raw materials and CO<sub>2</sub> emissions from the construction industry has been strongly anchored in various European directives. The Roadmap to a Resource Efficient Europe COM (2011) 571 [8] and the Eco-Innovation Action Plan (Eco-AP) COM (2011) 899 [9] both highly promote recycling and reuse of waste. Wastes (or by-products) would be incorporated in cement in two stages: (i) in the raw meal of clinker as a source of aluminium and iron or (ii) as a hydraulic or pozzolanic mineral additive (supplementary cementitious material) as reactive components at the later stage of the production [10,11]. Belite-sulfoaluminate cement (BCSA) is a potentially more environmentally friendly alternative cementitious binder to OPCs, as the CO<sub>2</sub> emissions during production are 20–30% lower than that of OPC clinker production [11]. The main advantages of BCSAs are that their production requires a significantly lower limestone amount, reduced energy for grinding, and lower clinkering temperatures ensuring still a broad range of compositions' possibilities. Such clinkers are generally produced by burning raw materials like limestone, clay, and bauxite in addition to calcium sulfate within a temperature (T) range of 1250 °C to 1350 °C [12]. With respect to OPC, BCSA clinkers have different phase assemblage, and the main phases are belite (C<sub>2</sub>S) which is usually in the range of 40–70 wt. %, calcium sulfoaluminate (C<sub>4</sub>A<sub>3</sub>S) in 20–40 wt. %, and ferrite (C<sub>4</sub>AF) which contents vary from 10 to 25 wt. % [11,13,14]. Besides, it may also contain other minor phases, such as mayenite, gehlenite, perovskite, and periclase [15,16]. The BCSA cements are prepared by adding varying amounts of calcium sulfate [17,18] whereas the main hydration products are calcium silicate hydrates (C–S–H), ettringite, monosulfate, aluminium hydroxide, and strätlingite [13]. The significant advantage of BCSAs is their potential for incorporation of various secondary raw materials rich in Al<sub>2</sub>O<sub>3</sub>, CaO, SiO<sub>2</sub>, and Fe<sub>2</sub>O<sub>3</sub> that are currently landfilled and represent a challenging environmental problem [7]. Industrial wastes (by-products) like bottom ash [19], steel slag [20] and fly ash [21] have been used as secondary raw materials for BCSA clinker synthesis, but also mine and quarry wastes show the great potential. Mine and quarry waste such as stockpiles of sub-ore, marginal ore, waste rock or tailings are typically rich in oxides of silicon, aluminium, calcium, and iron [22] which are also the main constituents of BCSA clinker and cement. There is a substantial sample of papers that have examined the possibilities to use phosphate rocks [23], Pb-Zn ore tailings [24], aluminium tailings, and aluminium ore waste rock [25], but little information on the utilization of limestone quarry waste for synthesis low CO<sub>2</sub> cements, especially BCSA. This research aimed to examine the potential of incorporating selected mine and quarry waste into cement clinker raw mixtures as secondary raw materials (SRM) to produce sustainable belite-sulfoaluminate cement (BCSA). The SRM included two types of quarry waste and one type of mine waste collected as part of the RIS ALiCE project [10,26] in Slovenia and Serbia. Detailed mineralogical, chemical, and radiological characterization of the raw materials was conducted followed by characterizing the phase composition of the cement using X-ray powder diffraction (XRD), thermal analysis (DTA/TG), and isothermal calorimetry. Finally, the compressive strength of the cement pastes according to the type of SRM incorporated into the clinker raw mixture was determined.

## 2. Materials and Methods

### 2.1. Materials

The clinker raw mixtures incorporating waste samples (two types of limestone quarry waste and mine waste) were prepared with limestone, flysch, gypsum, and bauxite. For the correction of the chemical composition to the targeted phase composition, smaller quantities of mill scale were used. Waste samples were collected from mineral waste

materials produced in three different active mine sites; a limestone aggregate quarry (W1), a limestone quarry for the production of calcium carbonate powders (W2), and a Pb-Zn mine (W3).

W1 represents unprocessed clay with blocks and gravel of limestone—mainly overburdened and heterogeneous material from karstic cavities which are not suitable for the production of limestone aggregates. W2 was collected from rejected material with grain diameters  $< 45 \mu\text{m}$  during wet separation, where limestone grains suitable for processing into calcium carbonate powder are separated from clay minerals, iron oxides, and fine-grained limestone. The waste material is then filter pressed and stockpiled. W3 represents mining waste from the Pb-Zn mine consisting mainly of schists and gneiss rock, with the presence of sulphide ore minerals such as galena, sphalerite, and chalcopyrite.

The mine waste samples were collected in 2019. Each sample was composed of at least 10 subsamples randomly collected from the surface of different parts of the mine waste deposit or the current stockpile. The weight of each composite sample was approximately 50 kg. All samples of raw materials for the synthesis of cement clinker were dried at  $105^\circ\text{C}$  to constant mass, except white titanogypsum, which was dried at  $40^\circ\text{C}$  to prevent dehydration. Each raw material was after drying milled in a ball mill until it met the criteria that 95 wt. % of the material could pass through a  $200 \mu\text{m}$  sieve.

The proportion of raw materials in the clinker raw mixtures (K1, K2, and K3) are presented in Table 1 as calculated using the Bogue method for sulfoaluminate cements [27]. The main oxide composition and loss on ignition at  $950^\circ\text{C}$  of the raw materials for the synthesis of cement clinker are described by Žibret et al. [20].

**Table 1.** Clinker raw mixtures (wt. %).

Clinker	Limestone	Flysch	W1	W2	W3	Gypsum	Bauxite	Mill Scale	Sum
K1	63.83	0.00	27.97	0.00	0.00	3.71	4.07	0.42	100.00
K2	0.00	47.75	0.00	43.22	0.00	3.78	4.80	0.45	100.00
K3	56.10	24.01	0.00	0.00	10.49	3.83	5.57	0.00	100.00

The synthesis and sintering ( $1250^\circ\text{C}/60 \text{ min}$ ) of the cement clinkers are described by Žibret et al. [20].

The targeted phase composition of the clinker raw mixtures was 65 wt. % belite, 20 wt. % calcium sulfoaluminate and 10 wt. % ferrite, while the actual phase composition of the synthesized clinkers derived from quantitative X-ray diffraction (PANalytical Empyrean X-ray diffractometer, Malvern Panalytical, Malvern, UK) is given in Table 2. X-ray diffraction patterns of clinkers K1, K2, and K3 are shown in Figure 1. Besides main clinker phases (calcium sulfoaluminate, belite, and ferrite), also minor phases such as mayenite, gehlenite, periclase, perovskite, arcanite, and aphtitalite formed. The phase composition of the K3 clinker sample is the closest to the targeted phase composition.

**Table 2.** The phase composition of the sintered clinkers (wt. %).

Phase Composition	K1	K2	K3
Calcium sulfoaluminate	17.3	15.8	22.6
Belite	69.1	71.4	64.8
Mayenite	1.7	1.4	0.4
Ferrite	8.9	4.9	9.0
Gehlenite	0.4	1.5	0.0
Periclase	1.1	1.1	1.2
Perovskite	0.0	1.4	1.2
Arcanite	1.0	1.1	0.2
Aphthitalite	0.5	1.4	0.6
Sum	100.0	100.0	100.0

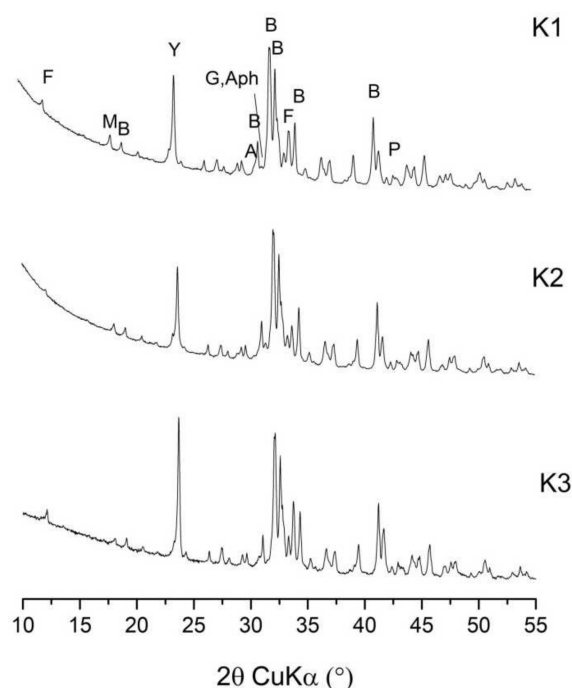


**Figure 1.** X-ray diffraction patterns of clinkers K1, K2, and K3. B—belite, Y—calcium sulfoaluminate, F—ferrite, G—gehlenite, P—periclase, Aph—aphtthitalite, A—arcanite, M—mayenite.

The cements were prepared from clinkers and white titanogypsum. Clinkers were ground using a laboratory disc mill such that they could pass through a 125  $\mu\text{m}$  sieve. According to the type of waste, the cements were labeled as follows: C1 from the W1 waste; C2 from the W2 waste, and C3 from the W3 waste. Gypsum was blended with the ground clinkers in a gypsum/calcium sulfoaluminate molar ratio of 1.5 (based on the actual amount of calcium sulfoaluminate determined by the Rietveld method, the gypsum content was 7.14, 6.69 and 9.03 wt. % for C1, C2, and C3, respectively). The prepared cements were homogenized in a Turbula for 1.5 h and further milled to a similar Blaine specific surface area (SSA) of  $4800 \pm 150 \text{ cm}^2/\text{g}$ . The particle size distribution (PSD) of the cements was measured using a Microtrac SYNC (Model 5001, Microtrac Retsch GmbH, Haan, Germany; dry operation), as is shown in Table 3.

**Table 3.** Results of laser granulometry analysis for the three cements ( $\mu\text{m}$ ).

Cement	D <sub>10</sub>	D <sub>50</sub>	D <sub>90</sub>
C1	1.46	8.60	44.03
C2	1.38	14.48	57.07
C3	1.34	7.31	44.89

## 2.2. Methods

### 2.2.1. Chemical and Mineralogical Characterization of the SRM

The main oxides ( $\text{SiO}_2$ ,  $\text{Al}_2\text{O}_3$ ,  $\text{Fe}_2\text{O}_3$ ,  $\text{CaO}$ ,  $\text{SO}_3$ ,  $\text{MgO}$ ,  $\text{Na}_2\text{O}$ ,  $\text{K}_2\text{O}$ ,  $\text{Cl}^-$ ) and LOI 950  $^\circ\text{C}$  were determined according to EN 196-2 [28]. The contents of  $\text{Cr}_2\text{O}_3$ ,  $\text{P}_2\text{O}_5$ ,  $\text{MnO}$ , and  $\text{TiO}_2$  were determined using a Wavelength Dispersive X-ray Fluorescence (WD XRF) analyzer produced by Thermo Scientific ARL Perform X. Before each measurement, a fused bead was prepared with a mixture of the sample and flux (Lt66:LM34 + 0.2% LiBr) in a ratio of 1:10, heated at 1050  $^\circ\text{C}$ .

In sample W3 trace elements (TE) and the content of rare earth elements (REE) were determined by an ICP-OES (Perkin Elmer Avio200 ICP-OES, Waltham, MA, USA) instrument with an S10 autosampler, MiraMIST nebulizer, glass baffled cyclonic spray chamber and

lutetium as the internal standard. Sample preparation included grinding to under 1 mm and fusion with lithium metaborate (0.5 g sample + 1.16 g lithium metaborate + 0.05 g  $\text{NH}_4\text{NO}_3$ ) at 1000 °C (1 h) in a platinum crucible [29]. The TE and REE of samples W1 and W2 were determined by an Ultra-trace ICP-ES/MS (MA250, Vancouver, BC, Canada), where a 0.25 g split is heated in  $\text{HNO}_3$ ,  $\text{HClO}_4$ , and HF to fuming, taken to dryness, and then the residue dissolved in HCl.

Mercury was determined by a mercury analyzer (AMA 254 Advanced Mercury Analyzer, LECO Corporation, St. Joseph, MI, USA).

The mineralogical composition of the mine and quarry waste samples was determined using a PANalytical Empyrean X-ray diffractometer (Malvern Panalytical, Malvern, UK) equipped with  $\text{CuK}\alpha$  radiation and a PIXcel 1D detector. Samples were ground in an agate mortar to a particle size below 0.063 mm. The ground powders were manually back-loaded into circular sample holders (27 mm in diameter) and data for each sample were collected from 4° to 70° (2 $\theta$ ) using a step size of 0.026° 2 $\theta$  with a scan step time of 397 s. Samples were measured at 45 kV and 40 mA and rotated during data collection with a revolution time of 2 s. The amount of crystalline phase and amorphous phase was estimated by Rietveld refinement using the external standard method (pure corundum,  $\text{Al}_2\text{O}_3$ ; NIST 6769) and PANalytical X'Pert High Score Plus diffraction software, using the structures for the phases from ICDD PDF 4 + 2016 RDB powder diffraction files.

#### 2.2.2. Radiological Characterization of SRM

Gamma-ray spectrometry was used to determine the activity concentration of radionuclides in quarry and mine waste as raw materials in the production of clinker. Six weeks before measurements the samples were put in plastic circle moulds to get to the radioactive equilibrium. A coaxial semiconductor high purity germanium (HPGe) detector (Canberra, Meriden, CT, USA) associated with standard beam supply electronics units for radiological measurements was realized [30]. According to laboratory standards, a certified radioactive solution purchased from the Czech Metrology Institute for calibrating the energy and efficiency of the spectrometer was used [31]. The efficiencies obtained were corrected for a coincidence summing effect using correction factors obtained from EFTRAN software [32]. The radioactivity measurement in our earlier publication was described [33].

#### 2.2.3. Characterization of the Cements

The hydration experiments of prepared cements were performed at 20 °C using a water to cement ratio of 0.5. At 28 days, prior to X-ray diffraction analysis and differential thermal analysis/thermogravimetric analysis (DTA/TG), hydration of the cement pastes was stopped by solvent exchange with isopropanol, in line with the recommendation by Snellings et al. [34]. The samples were ground to a particle size of below 63  $\mu\text{m}$ .

The phase composition of the cement pastes was determined using a PANalytical Empyrean X-ray diffractometer (Malvern Panalytical, Malvern, UK) equipped with  $\text{CuK}\alpha$  radiation and a PIXcel 1D detector. Samples were manually back-loaded into a circular sample holder (diameter 10 mm) to reduce the possible preferred orientation. The samples were measured at 45 kV with a current of 40 mA, in the 2 $\theta$  range from 4 to 70°, using a step size of 0.026° 2 $\theta$  with a scan step time of 297 s. Analysis of the X-ray diffraction patterns was performed using X'Pert High Score Plus diffraction software (v.4.9) from PANalytical (Malvern, UK), using PAN ICSD v. 3.4 powder diffraction files. The Rietveld refinement method was conducted using crystal structures by Snellings et al. [35]. The structures for cubic and orthorhombic calcium sulfoaluminate were as used by Cuesta et al. [15,36].

DTA/ TG measurements on the cement pastes were performed by Netzsch STA 409 instrument (Netzsch-Gerätebau GmbH, Selb, Germany). The measurements were conducted in the temperature interval from 30 to 1000 °C, with a heating rate of 100/min under a nitrogen atmosphere (flow speed of 20 mL/min). The samples (20 mg) granulated to less than 63  $\mu\text{m}$  were placed in alumina crucibles. Netzsch Proteus Thermal Analysis (Netzsch-Gerätebau GmbH, Selb, Germany) software was used for the data analysis.



Isothermal conduction calorimetry (TAM Air 8 calorimeter—TA Instruments) was employed to monitor the hydraulic reactivity of the cements. A total of 12 g of cement, previously ground to below 0.125 mm, was mixed using a water/ cement ratio of 0.5. A total of 6 g of mixed paste was then placed into glass vials and immediately placed into the calorimeter. The heat evolution of the cement was evaluated for 7 days at 20 °C.

The compressive strength was determined on the cement pastes samples with a water/cement ratio ( $w/c$ ) of 0.5 were poured into prismatic moulds with dimensions of  $10 \times 10 \times 25 \text{ mm}^3$ . After 24 h the cement paste samples were demoulded and cured in sealed plastic bags under laboratory conditions at  $T 21 \pm 2 \text{ °C}$  and 95% relative humidity until being tested under laboratory conditions. The compressive strength of the cement pastes was determined after 28 days, using a ToniNORM test device (ToniTechnic by ZwickRoell Group, Ulm, Germany) at a load rate of 0.05 kN/s. Results are given as the average of four measurements for each cement mixture.

### 3. Results and Discussion

#### 3.1. Characterization of the Secondary Raw Materials

##### 3.1.1. Mineralogical Composition

Analyzing the mineralogical composition of diverse mining wastes reveals the presence of several phases, including aluminosilicates, carbonates, silicates, and iron oxide phases [37].

Table 4 presents the mineral composition of the secondary raw materials. Quartz, calcite, and clay minerals (illite/muscovite, kaolinite, clinoclhorite) are the dominant minerals in the W1 sample, while dolomite is also present in a minor amount. Calcite is the predominant mineral in the W2 sample. The primary crystalline phases identified in the mine waste (W3) are quartz and chlinochlore, followed by calcite, muscovite, feldspar, and pyrite. Compared to the other two samples, the amount of amorphous phase was considerably lower in W2.

**Table 4.** Mineralogical composition of the waste samples (wt. %).

Sample	Amorphous		Crystalline								Sum
	Q	C	I/M	K	F	Chl	D	P	H	S	
W1	42.3	21.1	16.6	16.0	2.6	-	1.1	0.3	-	-	100.00
W2	2.8	0.1	96.2	-	-	-	0.9	-	-	-	100.00
W3	32.9	23.8	9.3	5.3	-	4.8	22.3	1.2	0.3	0.1	100.00

Q-quartz; C-calcite; I/M-Illite/Muscovite; K-kaolinite; F-feldspar; Chl-clinochlore; D-dolomite; P-pyrite; H-hornblende; S-sphalerite.

##### 3.1.2. Major Oxides

The chemical composition of the secondary raw materials is presented in Table 5. The two quarry wastes have different chemical compositions, which are connected to their origin and processing. Clay-rich waste in the W1 sample showed a high level of silica ( $\text{SiO}_2$ ), medium alumina content ( $\text{Al}_2\text{O}_3$ ), and a low level of iron oxide ( $\text{Fe}_2\text{O}_3$ ). Relatively high levels of CaO, combined with the loss of ignition (LOI at 950 °C) values, show the considerable presence of calcite. CaO was the major oxide in the sample W2 which indicates that the material consists of almost purely calcite, which was confirmed by analysis of the mineralogical composition (as described above). The W3 mineral waste is rich in  $\text{SiO}_2$ ,  $\text{Al}_2\text{O}_3$ , CaO, and  $\text{Fe}_2\text{O}_3$ , making it an attractive resource of oxides which are the main constituents used in the production of cement.

**Table 5.** Chemical composition of the secondary raw materials, wt. %.

Sample	LOI	SiO <sub>2</sub>	Al <sub>2</sub> O <sub>3</sub>	Fe <sub>2</sub> O <sub>3</sub>	CaO	MgO	SO <sub>3</sub>	Cl <sup>−</sup>	Na <sub>2</sub> O	K <sub>2</sub> O	P <sub>2</sub> O <sub>5</sub>	TiO <sub>2</sub>
W1	16.17	45.29	14.72	5.15	13.60	1.62	0.12	0.008	0.12	1.84	0.11	0.81
W2	42.70	1.01	1.01	0.17	53.61	0.91	0.09	0.002	0.01	0.02	<0.01	0.02
W3	5.54	48.98	11.61	11.62	9.15	2.58	0.07	0.009	0.47	1.84	0.41	0.85

Concerning the targeted phase compositions of the cement clinker, it was possible to incorporate 27.96 wt. %, 43.22 wt. %, and 10.43 wt. %, of clay residue, calcite residue, and mine waste, respectively, thus replacing the natural raw materials of the cement clinker raw mixture. Comparing the chemical compositions of the W1 and W3 wastes, which differed in origin, it can be seen that, except for the Fe<sub>2</sub>O<sub>3</sub> content, the chemical composition of the basic oxides dominant in the synthesis of clinker minerals was similar. In Pb-Zn waste, due to the high Fe<sub>2</sub>O<sub>3</sub> content, less waste was incorporated into the clinker.

CaO, SiO<sub>2</sub>, Al<sub>2</sub>O<sub>3</sub>, SO<sub>3</sub>, and Fe<sub>2</sub>O<sub>3</sub> are the main constituents in clinker related to targeted phase composition. MgO, alkalis, TiO<sub>2</sub>, P<sub>2</sub>O<sub>5</sub>, SO<sub>3</sub>, and Cl, as minor components, also could have an influence (depending on their content) on the clinker formation in the burning process and the process of cement hydration [38]. The MgO content ranges between 0.91 wt. % and 2.58 wt. %. A higher MgO content in the raw mixture can, however, result in the formation of periclase. The values are below the limit for the requirements for OPC clinker, which stipulate that the MgO content should not exceed 5 wt. % [39].

In any case, the chloride contents are relatively low, given that, according to EN 197-1 [39], the amount of Cl<sup>−</sup> in cement should not exceed 0.10 wt. %.

### 3.1.3. Trace Elements

Results from the elemental analysis of trace elements are presented in Table 6. This is clearly reflected in their elemental composition, which is comparable to the composition of soils and sediments that have developed on carbonate rocks [40]. The composition of sample W3 differs significantly from W1 and W2. Considering that this sample represents mine waste from a Pb-Zn mine, elevated levels of Pb and Zn were both expected and detected. Interestingly, this sample also has elevated levels of Mn. Pb has the retarder effect in OPC. It reduces the strength of cement paste moderately when 0.5 wt. % Pb is used and incorporated into the structure of C-S-H [41]. In relation to Zn, it has no influence on the properties of cement as it is incorporated in clinker minerals. The amounts of ZnO in a raw mixture is essential to ensure the whole incorporation of ZnO into the clinker minerals, thus decreasing the amount of ZnO to transfer to free ZnO. The presence of free ZnO (zincite) could cause serious damage to early hardening, leading to retardation of setting and a decrease of early strength [42]. Mn and Zn improve the burnability of clinker but decreased slightly the grindability of the clinker. During clinkering process, MnO replaces iron thus influencing the clinker and cement properties [42]. Like in OPC, heavy metal ions are more likely dissolved in sulfoaluminate clinker phases [43,44], thus targeted composition of clinker (incorporating 10.43 wt. % of Pb-Zn mine waste) is expected to have no significant influence on the clinker or cement properties. The use of large proportions of such mine waste in cement clinker production may increase the total content of these elements in the clinker, but it is unlikely to exceed regulatory limits or present a risk of leaching of the elements, as shown in Argane et al. [45] where material with similar composition was used.

The content of volatile elements is low in all three samples. It would not increase their usual emissions to the atmosphere.

The Chromium (VI) Directive (2003/53/EC) [46] limits the level of soluble Cr(VI) to a maximum of 2 ppm by mass of cement when water is added.

**Table 6.** Results showing the trace/heavy elements in the waste samples, [mg/kg].

Trace/Heavy Elements	W1	W2	W3
Ag	0.034 *	0.035 *	b.q.l.
As	21.2	4.1	34.7
Ba	249	11.0	513
Be	3.0	<1	3.3
Cd	0.5	0.5	9.9
Co	18.3	0.6	12.9
Cr	88.0	8.0	118
Cu	24.6	4.4	101
Ga	18.4	0.9	b.q.l.
Hg	0.169	0.026	0.025
Li	69.5	2.1	n.d.
Mn	353	54	10,672
Nb	10.0	0.6	b.q.l.
Ni	63.2	2.8	77.6
Pb	26.3	7.4	3217
Sb	1.5	0.2	b.q.l.
Se	0.5	<0.3	n.d.
Sr	74.0	116	274
Ta	0.7	<0.1	b.q.l.
Th	10.7	0.9	b.q.l.
Ti	0.9	0.1	n.d.
U	2.7	0.2	b.q.l.
V	121	3.0	103
Zn	98.6	13.5	2189
Zr	67.0	5.3	150

Remark: Sample W3: Selenium and Thallium failed in the recovery test, so these values are not given (marked as n.d.); b.q.l.—below quantification level; \* units µg/kg.

### 3.1.4. Rare Earth Elements

Analysis of the REE content shows that the W2 sample is depleted of REEs, while samples W1 and W3 have REE levels comparable to the upper Earth's crust [47]. The fact that the W2 sample is depleted of REEs is most likely a reflection of the overall depletion of REEs in the lithological unit extracted from that location (i.e., middle and upper Triassic limestone). Based on the results, shown in Table 7, the extraction of REEs from these materials is not feasible.

**Table 7.** The content of REEs in the three mine waste samples, [mg/kg].

Sample	Light REE									Heavy REE						
	Ce	Eu	Gd	La	Nd	Pr	Sm	Sc	Dy	Er	Ho	Lu	Tb	Tm	Yb	Y
W1	64.4	0.9	4.6	30.9	26.8	6.8	5.3	14.0	3.7	1.6	0.7	0.2	0.6	0.3	2	19.1
W2	5.0	<0.1	0.5	2.9	2.4	0.5	0.4	0.6	0.5	0.1	0.1	<0.1	<0.1	<0.1	0.3	2.4
W3	50.6	<5.0	<15	27.4	22.8	<15	<7.5	9.5	<7.5	<7.5	<7.5	*	<7.5	<7.5	<2	18.7

\* Lutetium was used as an internal standard, so was not measured in these samples.

### 3.1.5. Radiological Characterization

Results from the gamma spectrometric analysis of all samples are given in Table 8, with dose calculations being performed based on these values. In W1, W2, and W3 samples natural radionuclides <sup>238</sup>U, <sup>235</sup>U, <sup>226</sup>Ra, <sup>232</sup>Th, <sup>210</sup>Pb, and <sup>40</sup>K and artificial radionuclide <sup>137</sup>Cs were detected. The concentrations of <sup>137</sup>Cs were <0.2 Bq/kg for W3 and <0.04 and 0.03 Bq/kg for W1 and W2 samples respectively. According to UNSCEAR 2000 [48], the Earth's crust contains between 0.5 and 5 ppm of uranium, with a <sup>235</sup>U and <sup>238</sup>U isotope activity ratio of about 0.04. In the examined samples, the ratio of <sup>235</sup>U and <sup>238</sup>U is close to this value and within the limits of measurement uncertainties.



**Table 8.** Activity concentration of the natural radionuclides and  $^{137}\text{Cs}$ .

Sample	Activity Concentration, [ $\text{Bq}\cdot\text{kg}^{-1}$ ]							
	$^{210}\text{Pb}$	$^{226}\text{Ra}$	$^{232}\text{Th}$	$^{40}\text{K}$	$^{137}\text{Cs}$	$^{238}\text{U}$	$^{235}\text{U}$	$^{235}\text{U}/^{238}\text{U}$
W1	$51.4 \pm 6.1$	$41.2 \pm 2.7$	$41.8 \pm 3.1$	$568.0 \pm 3.1$	$<0.04$	$56.6 \pm 6.4$	$2.5 \pm 0.4$	0.044
W2	$<1$	$<10.0$	$2.3 \pm 0.4$	$18.0 \pm 1.9$	$<0.03$	$3.1 \pm 1.0$	$<0.2$	$<0.065$
W3	$17.6 \pm 3.3$	$34.0 \pm 2.0$	$15.0 \pm 2.0$	$345.0 \pm 25.0$	$<0.2$	$19.3 \pm 4.7$	$1.3 \pm 0.2$	0.067

In W2 and W3 the activity concentrations of  $^{238}\text{U}$  are below the world average value [48]. There are great differences between the activity concentrations of radionuclides in the two different quarry wastes, which is presumably the result of very different mineral compositions of W1 and W2 samples (Table 4). The detected mean activity concentrations of  $^{40}\text{K}$ ,  $^{232}\text{Th}$ , and  $^{226}\text{Ra}$  in W1 sample were higher than their world average values for building materials [48]. Uranium is more mobile than thorium and moves easily through the crystal lattices of minerals present in the investigated samples. Due to the difficult migration thorium is retained in some minerals that are present in the samples measured [49]. However, the activity concentration of  $^{232}\text{Th}$  in all investigated samples is slightly lower compared to  $^{238}\text{U}$ , but the activity concentration of both radionuclides exceeds the world average value for sample W1 [48].

#### Dose Calculations

The assessment of the radiation risk from the use of construction materials can often be performed with several adopted dimensionless quantities, the so-called “Hazard index” representing the measure of the possibility of radiological hazard. In our research, as a first, we focused on the calculation of the gamma activity concentration index ( $I$ ), which only be used as a screening tool for materials that potency be of interest for utilizing in the construction sector. The European Commission [50] was proposed this index and calculated using the following equation:

$$I = A_{\text{Ra}}/300 \text{ Bqkg}^{-1} + A_{\text{Th}}/200 \text{ Bqkg}^{-1} + A_{\text{K}}/3000 \text{ Bqkg}^{-1} \quad (1)$$

where  $A_{\text{Ra}}$ —specific activities of  $^{226}\text{Ra}$ ;  $A_{\text{Th}}$ —specific activities of  $^{232}\text{Th}$ ; and  $A_{\text{K}}$ —specific activity of  $^{40}\text{K}$ .

Gamma index is correlated with an annual dose rate. Besides dose criteria, the quantity and type of the material influence the limit values of the gamma index of materials which is used in construction. For material used in bulk  $I \leq 1$  corresponds to an absorbed gamma dose rate of 1 mSv per year [50] which is the highest dose rate value recommended for the population [48]. It is estimated that about 65 wt. % of the population receives a dose between 1 mSv and 3 mSv per year, about 25 wt. % receive doses less than 1 mSv, while for 10 wt. % of the population the annual doses are above 3 mSv. Radiological measurement is necessary to estimate whether the used waste material meets all the law regulations for it to be used as a component of clinker mixture in cement production. To estimate the potential influence on health after exposure to natural radionuclides present in the samples, the radium equivalent activity,  $Ra_{\text{eq}}$  ( $\text{Bq kg}^{-1}$ ), the external hazard index,  $H_{\text{ex}}$  ( $\text{Bq kg}^{-1}$ ), the total external absorbed gamma dose rate,  $\dot{D}$  ( $\text{nGy/h}$ ), and the annual effective dose rate,  $EDR$  ( $\text{mSv y}^{-1}$ ), were calculated. The equations for their calculation that were used originate from the cited literature [50].

Table 9 shows values of the gamma index, the radium equivalent activity, external radiation hazard index, external absorbed dose rate, and annual effective dose rate calculated for all of the investigated samples.

**Table 9.** Gamma index, radium equivalent activity, external radiation hazard index, external absorbed dose rate and annual effective dose rate, and of the all investigated samples.

Sample	Gamma index <i>I</i>	$Ra_{eq}$ [Bqkg <sup>-1</sup> ]	$H_{ex}$ [Bqkg <sup>-1</sup> ]	$\dot{D}$ [nGyh <sup>-1</sup> ]	EDR [mSvy <sup>-1</sup> ]
W1	0.54	145	0.409	129	0.634
W2	0.02	14.7	0.040	13.2	0.645
W3	0.30	96.3	0.271	86.4	0.423

The values of the Gamma index of the tested samples are lower than the recommended value of 1. Since these samples are used as secondary raw materials in raw mixtures of cement clinker, it will not raise the index-I of the final product above 1, so the dose rate will not exceed 1 mSv per year. According to the obtained results related to the gamma index, these types of waste materials can be used as raw materials in the production of cement from a radiological point of view.

In sample W2, the value of the absorbed dose rate,  $\dot{D}$  is much lower than the world population-weighted average for the indoor absorbed gamma dose rate (84 nGy h<sup>-1</sup>), whereas in sample W3 it is slightly higher. The results show the radium equivalent activity of all the samples varied from 14.7 to 145 Bq/kg. The calculated values are lower than the recommended safe limit of 370 Bq/kg [50]. To provide the safe utilization of SRM as a component of clinker mixture, and to retain the radiation hazard inconsiderable, the value of  $H_{ex}$  should be less than unity [50]. As shown, in all samples the values of  $H_{ex}$  are lower than the recommended safe limit, indicating that their radiation hazard is insignificant and that they are safe to be used in the production of cement.

The values of investigated indices relating to the activity concentration, gamma absorbed dose rate, radium equivalent activity, annual effective dose and radiological hazard of SRM are comparable to the average ranges worldwide, although a few of the radiological parameters measured are higher than the permissible limits (refers to the sample W1).

### 3.2. Characterization of Cement

#### 3.2.1. Phase Composition

The phase compositions of the cement pastes after 28 days of hydration, as determined by Rietveld refinement, are shown in Table 10. X-ray diffraction patterns of cement pastes C1, C2, and C3 at 28 days of hydration are shown in Figure 2. Figure 3 plots the DTA/TG results of the cement pastes after 28 days of hydration.

**Table 10.** The phase composition of the cement pastes after 28 days of hydration, as determined by Rietveld refinement (wt. %).

Phase Composition	C1	C2	C3
Σ Calcium sulfoaluminate	0	0	0
Belite-beta	35.6	33.3	25.7
Belite-gamma	4.1	4.4	5.8
Σ Belite	39.7	37.7	31.5
Mayenite	0.0	0.0	0.0
Ferrite	2.0	0.0	1.6
Gehlenite	0.6	1.1	0.0
Perovskite	0.1	0.7	0.0
Periclase	0.3	0.4	0.0
Ettringite	13.0	11.6	19.5
Monosulfate	1.9	2	0.6
Strätlingite	0.9	2.2	0.1
Amorphous	41.5	44.3	46.7
Sum	100.0	100.0	100.0

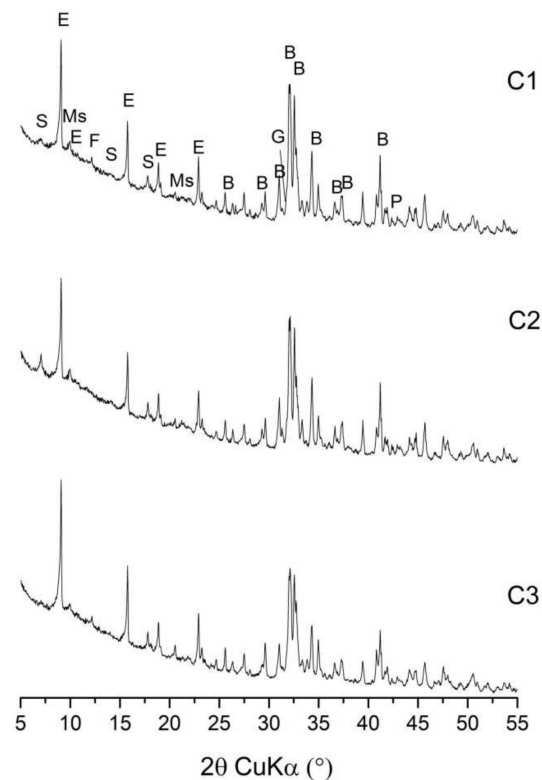


**Figure 2.** X-ray diffraction patterns of cement pastes C1, C2, and C3 at 28 days of hydration. B—belite, F—ferrite, G—gehlenite, P—periclase, E—ettringite, Ms—monosulfate, S—strätlingite.

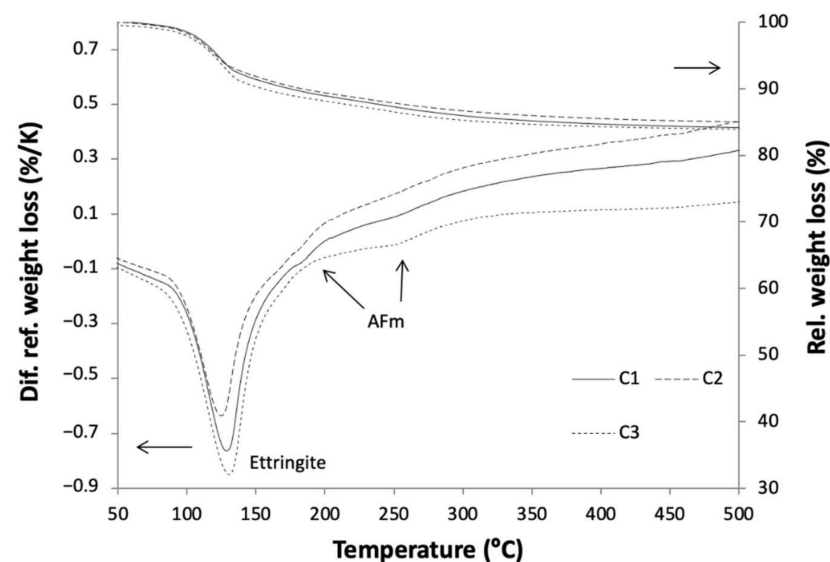


**Figure 3.** Thermogravimetric analysis of the cement pastes C1, C2, and C3 after 28 days of hydration.

The X-ray powder diffraction results show the presence of belite, ferrite, gehlenite, perovskite, and periclase as unhydrated phases and ettringite, monosulfate, and strätlingite as the main hydration products. In addition, an amorphous phase is present in the hydrated pastes. Calcium sulfoaluminate, gypsum, and mayenite were not detectable and must have already therefore been consumed. The amount of ettringite, which precipitates with the hydration of calcium sulfoaluminate [18,51], is controlled by the amount of calcium sulfoaluminate in the cement clinker mixture. Namely, when a higher amount of calcium sulfoaluminate is present, the formation of more ettringite, and consequently less monosul-

fate, is possible [52]. The amount of ettringite is highest in the cement paste C3, followed by C1, and the least in C2, as is in accordance with their calcium sulfoaluminate content. These results are consistent with thermogravimetric analysis, where weight loss attributed to the formation of ettringite can be seen around 120 °C [53]. When the calcium sulfate source is consumed, monosulfate is formed [54,55]. More monosulfate is present in C1 and C2, where less ettringite is present compared to C3. As a result of the hydration of belite with aluminium hydroxide, strätlingite is identified in all three samples [56]. The amount of strätlingite is lower in C3 due to the higher content of ettringite, which consumes the aluminium available for its formation [57]. The presence of AFm phases (monosulfate and strätlingite) is also confirmed by thermogravimetric analysis. The amorphous phase present is primarily attributed to C-S-H, as the main hydration product of belite.

### 3.2.2. Hydration Kinetics

The hydration heat of the cements analyzed is shown in Figure 4a. The results indicate that the kinetics of C1, C2, and C3 are slightly different.

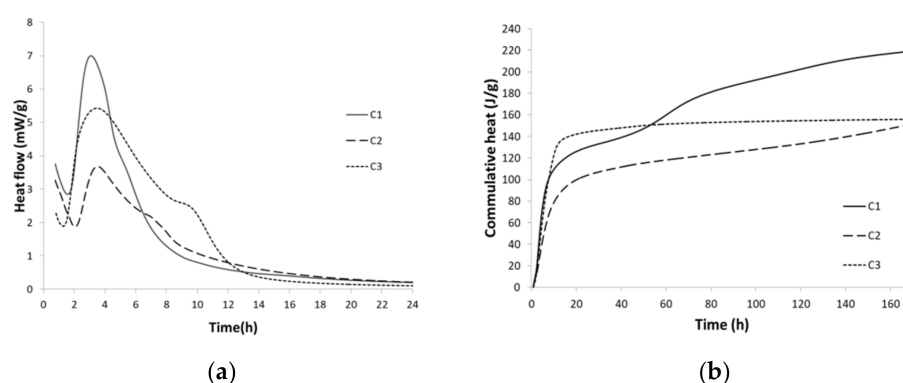


**Figure 4.** Hydration heat flow (a) of the C1, C2, and C3 cements and development of the cumulative heat of hydration (b).

The first peak, which is attributed to wetting and the early reaction during hydration [58–60], is missed due to the external mixing method. The results showed that samples C1 and C3 reacted slightly faster than C2 and had a shorter induction period. The induction period lasted around 1.8 h in C1 and C3 compared to 2 h in C2. C2 contained a lower amount of the highly reactive calcium sulfoaluminate phase and ferrite, which enhance reactivity, meaning it reacted the slowest. This sample also contained the highest amount of gehlenite, which reacts more slowly. Following the induction period, which is assigned to the dissolution of clinker phases and the early formation of ettringite [58,61], the main peak occurred, which is thereafter assigned to the formation of ettringite and aluminium hydroxide [18,61]. This exothermic peak occurred after around 3.8 h in all three samples. However, the most heat was released by C1, followed by C3, and the least by C2, in which the lowest amount of ettringite was detected by X-ray powder diffraction after 28 days of hydration. Furthermore, all samples displayed a small shoulder following the main peak, which occurred after 5.8 h, 7.5, and 10 h in C1, C2, and C3, respectively. This is attributed to the depletion of gypsum and the subsequent precipitation of monosulfate [58,61].

The cumulative heat results are presented in Figure 4b. The C3 samples showed significantly higher initial cumulative heat, ascribed to the higher calcium sulfoaluminate content in the cement clinker. This was followed by C1 and then C2, which has the lowest amount of calcium sulfoaluminate. At 7 days of hydration, the heat released was highest in C1 (220 J/g), while in C2 and C3 it was almost the same (155 J/g).

### 3.2.3. Compressive Strength

As seen from the results (Table 11) the compressive strength of the cement pastes varies according to the type of secondary raw material incorporated into the clinker raw mixture.

**Table 11.** Compressive strength of the cements after 28 days.

Sample	Compressive Strength (N/mm <sup>2</sup> )
C1	20.0 ± 0.9
C2	18.5 ± 1.3
C3	20.6 ± 1.0

The compressive strength was slightly lower in the C2 cement, which could be related to the lowest calcium sulfoaluminate content in this sample. In comparison to the other two cement mixtures, less gypsum was therefore needed in the mixture for an equal molar ratio.

The compressive strengths of the cements are comparable to the cements of similar clinker phase compositions, which is ascribed to the low content of calcium sulfoaluminate in cement [61] and consequently lower amount of precipitated ettringite [18].

Belite-rich BCSA cements in comparison to the calcium sulfoaluminate-rich BCSA cements showed lower compressive strength which is the consequence of the higher calcium sulfoaluminate content and a higher amount of precipitated ettringite present in calcium sulfoaluminate-rich BCSA [18]. However, due to the hydration of the belite phase and the formation of C–S–H, a significant increase in strength after 28 days is reported for those cements [62].

## 4. Conclusions

The present study investigated the potential to valorize quarry (clay and calcite residues) and mine (Pb–Zn) wastes in a belite-sulfoaluminate cement. Three types of BCSA clinker, with a targeted phase composition of 65 wt. % belite, 20 wt. % calcium sulfoaluminate and 10 wt. % ferrites, and sintered at 1250 °C/60 min, were studied. Various techniques were applied to characterize the waste, the clinkers, and the cements. In summary, the following conclusions were drawn:

- Following the concept of a circular economy, it is possible to use the investigated quarry and mine waste for the synthesis of belite-sulfoaluminate cement.
- Different experimental raw mixtures containing either 27.96 wt. % clay residue from a limestone quarry, 43.22 wt. % calcite residue from a limestone quarry, or 10.43 wt. % Pb–Zn mine waste were suitable for the synthesis of BCSA clinkers with targeted phase composition.
- Radiological characterization (I-index and dose assessment) of the quarry and mine wastes are mainly (except D) comparable to the average ranges worldwide. Generally, it can be concluded that all three wastes have a low impact from a radiological point of view, especially given that they are only used in a certain proportion of the final product.
- The hydraulic reactivity of cements, as evidenced by isothermal calorimetry, showed that C1 and C3 are slightly more reactive, with a shorter induction period in comparison to C2. The reactivity of cements is primarily connected to the highly reactive calcium sulfoaluminate phase (resulting in the formation of ettringite) and ferrite on one hand and the slowly reactive gehlenite on the other. In addition to the reactivity of the cement, the particle size distribution of the cements has also an impact (with  $D_{50}$  being lower in C1 and C3).
- The slightly higher reactivity of the C1 and C3 cements result in a slightly higher compressive strength in comparison to C2, which is connected to the chemical composition of the waste used.
- The present paper demonstrates the potential application of quarry (clay and calcite residues) and mine (Pb–Zn) wastes as raw materials in the production of BCSA cements.

**Author Contributions:** Conceptualization, S.D. and E.F.; methodology, S.D.; validation, S.D., E.F. and I.M.; investigation, K.Š., M.M., K.T. and S.D.; resources, K.Š., M.M., K.T. and G.Ž.; writing—original draft preparation, M.M., K.Š., K.T., G.Ž., M.F., B.P., I.M. and L.K.; writing—review and editing, S.D., E.F. and I.M.; supervision, I.M. and S.D.; project administration, S.D., E.F. and I.M.; funding acquisition, S.D. All authors have read and agreed to the published version of the manuscript.

**Funding:** The study has received funding from the European Institute of Innovation and Technology (EIT), a body of the European Union, under Horizon 2020, the EU Framework Programme for Research and Innovation (RIS-ALiCE, project no, 18258).

**Institutional Review Board Statement:** Not applicable.

**Informed Consent Statement:** Not applicable.

**Data Availability Statement:** Data is contained within the article.

**Acknowledgments:** The authors would like to thank Bence Kószó from Bay Zoltán Nonprofit Ltd. for Applied Research, Division for Biotechnology (BAY-BIO) H-6726 Szeged, Hungary for the ICP-OES analyses realized. The authors would also like to thank Ljubica Vladichevska from Cementarnica Usje A.D.-TITAN Group for all the useful comments relating to the influence of the chemical composition of secondary raw materials in cements, and Nikolina Stamatovska Aluloska for the Hg analysis. Additionally, the authors acknowledge the TU Wien Bibliothek for financial support through its Open Access Funding Program.

**Conflicts of Interest:** The authors declare no conflict of interest.

## References

- Available online: <https://www.iea.org/reports/global-status-report-for-buildings-and-construction-2019> (accessed on 15 February 2022).
- Miller, S.A.; Horvath, A.; Monteiro, P.J.M. Readily implementable techniques can cut annual CO<sub>2</sub> emissions from the production of concrete by over 20%. *Environ. Res. Lett.* **2016**, *11*, 074029. [CrossRef]
- Garside, M. Global Cement Production 1995–2020, Statista 2022. Available online: <https://www.statista.com/statistics/1087115/global-cement-production-volume> (accessed on 30 March 2022).
- Favier, A.; De Wolf, C.; Scrivener, K.; Habert, G. A Sustainable Future for the European Cement and Technology Assessment for Full Decarbonisation of The Industry by 2050, EPFL. Available online: [https://europeanclimate.org/wp-content/uploads/2018/10/AB\\_SP\\_Decarbonisation\\_report.pdf](https://europeanclimate.org/wp-content/uploads/2018/10/AB_SP_Decarbonisation_report.pdf) (accessed on 30 March 2022).
- Scrivener, K.L.; Vanderley, M.; John, V.M.; Ellis, M.; Gartner, E.M. Eco-efficient cements: Potential economically viable solutions for a low-CO<sub>2</sub> cement-based materials industry. *Cem. Concr. Res.* **2018**, *114*, 2–26. [CrossRef]
- Habert, G.; Miller, S.A.; John, V.M.; Provis, J.L.; Favier, A.; Horvath, A.; Scrivener, K.L. Environmental impacts and decarbonization strategies in the cement and concrete industries. *Nat. Rev. Earth Environ.* **2020**, *1*, 559–573. [CrossRef]
- Žibret, G.; Teran, K.; Žibret, L.; Šter, K.; Dolenec, S. Building of the Al-containing Secondary Raw Materials Registry for the Production of Low CO<sub>2</sub> Mineral Binders in South-Eastern European Region. *Sustainability* **2021**, *13*, 1535. [CrossRef]
- Roadmap to a Resource Efficient Europe COM(2011) 571. Available online: <https://eur-lex.europa.eu/legal-content/EN/TXT/?uri=CELEX:52011DC0571> (accessed on 15 February 2022).
- Thapa, V.B.; Waldmann, D.; Simon, C. Gravel wash mud, a quarry waste material as supplementary cementitious T material (SCM). *Cem. Concr. Res.* **2019**, *124*, 105833. [CrossRef]
- Dolenec, S.; Malovrh Rebec, K.; Lesek, A.; Šter, K.; Žibret, L.; Žibret, G.; Teran, K.; Pucko, E.; Merta, I.; Poletanovic, B.; et al. *Manual for Use of Al-Containing Residues in Low-Carbon Mineral Binders*; Slovenian National Building and Civil Engineering Institute: Ljubljana, Slovenia, 2020; p. 124. ISBN 978-961-94071-9-6.
- Gartner, E.; Sui, T. Alternative cement clinkers. *Cem. Concr. Res.* **2018**, *114*, 27–39. [CrossRef]
- Quillin, K. Performance of belite–sulfoaluminate cements. *Cem. Concr. Res.* **2001**, *31*, 1341–1349. [CrossRef]
- Bullerjahn, F.; Schmitt, D.; Ben Haha, M. Effect of raw mix design and of clinkering process on the formation and mineralogical composition of (ternesite) belite calcium sulfoaluminate ferrite clinker. *Cem. Concr. Res.* **2014**, *59*, 87–95. [CrossRef]
- Da Costa, E.B.; Rodríguez, E.D.; Bernal, S.A.; Provis, J.L.; Gobbo, L.A.; Kirchheim, A.P. Production and hydration of calcium sulfoaluminate–belite cements derived from aluminium anodising sludge. *Constr. Build. Mater.* **2016**, *122*, 373–383. [CrossRef]
- Álvarez-Pinazo, G.; Cuesta, A.; García-Maté, M.; Santacruz, I.; Losilla, E.R.; De la Torre, A.G.; León-Reina, L.; Aranda, M.A.G. Rietveld quantitative phase analysis of Yeelimite-containing cements. *Cem. Concr. Res.* **2012**, *42*, 960–971. [CrossRef]
- De la Torre, Á.G.; Cuberos, A.J.M.; Álvarez-Pinazo, G.; Cuesta, A.; Aranda, M.A.G. In situ powder diffraction study of belite sulfoaluminate clinkering. *J. Synchrotron Radiat.* **2011**, *18*, 506–514. [CrossRef] [PubMed]
- Glasser, F.P.; Zhang, L. High-Performance Cement Matrices Based on Calcium Sulfoaluminate–Belite Compositions. *Cem. Concr. Res.* **2001**, *31*, 1881–1886. [CrossRef]
- Mrak, M.; Winnefeld, F.; Lothenbach, B.; Dolenec, S. The influence of calcium sulfate content on the hydration of belite–calcium sulfoaluminate cements with different clinker phase compositions. *Mater. Struct.* **2021**, *54*, 212. [CrossRef]



19. Zibret, L.; Ipavec, A.; Dolenc, S. Microstructural characteristics of belite–sulfoaluminate cement clinkers with bottom ash. *Constr. Build. Mater.* **2022**, *321*, 126289. [\[CrossRef\]](#)
20. Žibret, L.; Šter, K.; Borštnar, M.; Lončnar, M.; Dolenc, S. The Incorporation of Steel Slag into Belite-Sulfoaluminate Cement Clinkers. *Appl. Sci.* **2021**, *11*, 1840. [\[CrossRef\]](#)
21. Kramar, S.; Žibret, L.; Fidanchevska, E.; Jovanov, V.; Angjusheva, B.; Ducman, V. Use of fly ash and phosphogypsum for the synthesis of belite-sulfoaluminate clinker. *Mater. Constr.* **2019**, *69*, 1–12. [\[CrossRef\]](#)
22. Gou, M.; Zhou, L.; Then, N.W.Y. Utilization of tailings in cement and concrete: A review. *Sci. Eng. Compos.* **2019**, *26*, 449–464. [\[CrossRef\]](#)
23. Li, R.; He, W.; Zhang, J.; Wang, Y.; Zhang, Y.; Nie, D. Preparation of belite–sulphoaluminate cement using phosphate rock acid-insoluble residue. *Constr. Build. Mater.* **2022**, *323*, 126573. [\[CrossRef\]](#)
24. Nouairi, J.; Hajjaji, W.; Costa, C.S.; Senff, L.; Patinha, C.; Ferreira da Silva, E.; Labrincha, J.A.; Rocha, F.; Medhioub, M. Study of Zn-Pb ore tailings and their potential in cement technology. *J. Afr. Earth Sci.* **2018**, *139*, 165–172. [\[CrossRef\]](#)
25. Chen, X.; Li, J.; Lu, Z.; Ng, S.; Niu, Y.; Jiang, J.; Xu, Y.; Lai, Z.; Liu, H. The Role of Brownmillerite in Preparation of High-Belite Sulfoaluminate Cement Clinker. *Appl. Sci.* **2022**, *12*, 4980. [\[CrossRef\]](#)
26. RIS-ALiCE Project, RIS-ALiCE: Al-Rich Industrial Residues for Mineral Binders in ESEE Region. Available online: <https://ris-alice.zag.si> (accessed on 15 February 2022).
27. Majling, J.; Strigáč, J.; RoY, D.M. Generalized Bogue computations to forecast the mineralogical composition of sulfoaluminate cements based on fly ashes. *Adv. Cem. Res.* **1999**, *11*, 27–34. [\[CrossRef\]](#)
28. EN 196-2; Method of Testing Cement—Part 2: Chemical Analysis of Cement. British Standards Institution: London, UK, 2013. Available online: <https://www.en-standard.eu/bs-en-196-2-2013-method-of-testing-cement-chemical-analysis-of-cement/> (accessed on 30 June 2013).
29. MSZ 525-17; Chemical Analysis of Cement. Part 17: Determination of Total Chrome Content as Cr<sub>2</sub>O<sub>3</sub>. Hungarian Standards Institution: Budapest, Hungary, 2013. Available online: [http://www.mszt.hu/web/guest/webaruhaz;jsessionid=F7A616D8B7651350184650DE1E6EC186?p\\_p\\_id=msztwebshop\\_WAR\\_MsztWApportlet&p\\_p\\_lifecycle=1&p\\_p\\_state=normal&p\\_p\\_mode=view&p\\_p\\_col\\_id=column-1&p\\_p\\_col\\_count=1&msztwebshop\\_WAR\\_MsztWApportlet\\_ref=157252&msztwebshop\\_WAR\\_MsztWApportlet\\_javax.portlet.action=search](http://www.mszt.hu/web/guest/webaruhaz;jsessionid=F7A616D8B7651350184650DE1E6EC186?p_p_id=msztwebshop_WAR_MsztWApportlet&p_p_lifecycle=1&p_p_state=normal&p_p_mode=view&p_p_col_id=column-1&p_p_col_count=1&msztwebshop_WAR_MsztWApportlet_ref=157252&msztwebshop_WAR_MsztWApportlet_javax.portlet.action=search) (accessed on 1 December 2013).
30. IAEA. *Measurement of Radionuclides in Food and the Environment*; Technical Report Series No. 295; IAEA: Vienna, Austria, 1989.
31. CMI. Radioactive Standard Solutions, ER X, Cert. No. 1035-SE-40844-17 Czech Metrology Institute Prague. 2017. Available online: <https://www.cmi.cz/Certificates%20of%20accreditation?language=en> (accessed on 1 January 2017).
32. Vidmar, T. EFFTRAN—A Monte Carlo efficiency transfer code for gamma-ray spectrometry. *Nucl. Instrum. Methods Phys. Res. Sect. A* **2005**, *550*, 603–608. [\[CrossRef\]](#)
33. Nenadović, S.; Fereone, C.; Nenadović, M.; Cioffi, R.; Mirković, M.; Vukanac, I.; Kljajević, L.J. Chemical, physical and radiological evaluation of raw materials and geopolymers for building application. *J. Radioanal. Nucl. Chem.* **2020**, *325*, 435–445. [\[CrossRef\]](#)
34. Snellings, R.; Chwast, J.; Cizer, O.; De Belie, N.; Dhandapani, Y.; Durdzinski, P.; Elsen, J.; Haufe, J.; Hooton, D.; Patapy, C.; et al. Report of TC 238-SCM: Hydration stoppage methods for phase assemblage studies of blended cements—Results of a round robin test. *Mater. Struct.* **2018**, *51*, 111. [\[CrossRef\]](#)
35. Snellings, R. X-ray powder diffraction applied to cement. In *A Practical Guide to Microstructural Analysis of Cementitious Materials*, 1st ed.; CRC Press: Boca Raton, FL, USA, 2016; pp. 126–195. [\[CrossRef\]](#)
36. Cuesta, A.; Alvarez-Pinazo, G.; Sanfelix, S.G.; Pearl, I.; Aranda, M.A.G.; De la Torre, A.G. Hydration mechanisms of two polymorphs of synthetic ye’elimite. *Cem. Concr. Res.* **2014**, *63*, 127–136. [\[CrossRef\]](#)
37. Mabroum, S.; Moukannaa, S.; El Machi, A.; Taha, Y.; Benzaazoua, M.; Hakkou, R. Mine wastes based geopolymers: A critical review. *Clean. Eng. Technol.* **2020**, *1*, 100014. [\[CrossRef\]](#)
38. Liu, X.; Li, Y. Effect of MgO on the composition and properties of alite-sulphoaluminate cement. *Cem. Concr. Res.* **2005**, *35*, 1685–1687. [\[CrossRef\]](#)
39. EN 197-1; Cement—Part 1: Composition, Specifications and Conformity Criteria for Common Cements. CEN: Brussels, Belgium, 2011.
40. Gosar, M.; Šajn, R.; Bavec, Š.; Gaberšek, M.; Pezdir, V.; Miler, M. Geochemical background and threshold for 47 chemical elements in Slovenian topsoil. *Geologija* **2019**, *62*, 7–59. [\[CrossRef\]](#)
41. Keppert, M.; Scheinherrová, L.; Jerman, M.; Doušová, B.; Kobera, L.; Brus, J.; Černý, R. Hydration of Ordinary Portland Cement in Presence of Lead Sorbed on Ceramic Sorbent. *Materials* **2019**, *12*, 19. [\[CrossRef\]](#)
42. Shimosaka, K.; Inoue, T.; Tanaka, H.; Kishimoto, Y. Influence of Minor Elements in Clinker on the Properties of Cement: A New Approach for Application to Commercial Cement Manufacturing. *Trans. Mater. Res. Soc. Jpn.* **2007**, *32*, 647–652. [\[CrossRef\]](#)
43. Zhu, J.; Chen, Y.; Zhang, L.; Yang, K.; Guan, X.; Zhao, R. Insights on Substitution Preference of Pb Ions in Sulfoaluminate Cement Clinker Phases. *Materials* **2021**, *14*, 44. [\[CrossRef\]](#) [\[PubMed\]](#)
44. Juenger, M.C.G.; Winnefeld, F.; Provis, J.L.; Ideker, J.H. Advances in alternative cementitious binders. *Cem. Concr. Res.* **2011**, *41*, 1232–1243. [\[CrossRef\]](#)
45. Argane, R.; Benzaazoua, M.; Hakkou, R.; Bouamrane, A. Reuse of base-metal tailings as aggregates for rendering mortars: Assessment of immobilization performances and environmental behavior, *Constr. Build. Mater.* **2015**, *96*, 296–306. [\[CrossRef\]](#)

46. EU Directive 2003/53/EC on Chromium in Cement. Directive 2003/53/EC of the European Parliament and of the Council of 18 June 2003 Amending for the 26th Time Council Directive 76/769/EEC Relating to Restrictions on the Marketing and Use of Certain Dangerous Substances and Preparations (Nonylphenol, Nonylphenol Ethoxylate and Cement). Available online: <http://eur-lex.europa.eu/LexUriServ/LexUriServ.do?uri=CELEX:32003L0053:en:NOT> (accessed on 30 March 2022).
47. Rudnick, R.L.; Gao, S. The Composition of the Continental Crust. In *The Crust*; Holland, H.D., Turekian, K.K., Eds.; Treatise on Geochemistry; Elsevier-Pergamon: Oxford, UK, 2003; Volume 3, pp. 1–64. [\[CrossRef\]](#)
48. UN Scientific Committee on the Effects of Atomic Radiation. *Sources and Effects of Ionizing Radiation, United Nations Scientific Committee on the Effects of Atomic Radiation, UNSCEAR 2008 Report to the General Assembly with Scientific Annexes*; United Nations: New York, NY, USA, 2010; ISBN 978-92-1-142274-0.
49. Gbenu, S.T.; Oladejo, O.F.; Alayande, O.; Olukotun, S.F.; Fasasi, M.K.; Balogun, F.A. Assessment of radiological hazard of quarry products from southwest Nigeria. *J. Radiat. Res. Appl. Sci.* **2016**, *9*, 20–25. [\[CrossRef\]](#)
50. European Commission. *Radiation Protection 112. Radiological Protection Principles Concerning the Natural Radioactivity of Building Materials*; Directorate-General Environment, Nuclear Safety and Civil Protection: Luxembourg, 1999; ISBN 92-828-8376-0.
51. Winnefeld, F.; Lothenbach, B. Hydration of calcium sulfoaluminate cements—Experimental findings and thermodynamic modelling. *Cem. Concr. Res.* **2010**, *40*, 1239–1247. [\[CrossRef\]](#)
52. Winnefeld, F.; Barlag, S. Calorimetric and thermogravimetric study on the influence of calcium sulfate on the hydration of ye’elimite. *J. Therm. Anal. Calorim.* **2010**, *101*, 949–957. [\[CrossRef\]](#)
53. Garcia-Mate, M.; De la Torre, A.G.; Leon-Reina, L.; Losilla, E.R.; Aranda, M.A.G.; Santacruz, I. Effect of calcium sulfate source on the hydration of calcium sulfoaluminate eco-cement. *Cem. Concr. Compos.* **2015**, *55*, 53–61. [\[CrossRef\]](#)
54. Winnefeld, F.; Martin, L.H.J.; Muller, C.J.; Lothenbach, B. Using gypsum to control hydration kinetics of CSA cements. *Constr. Build. Mater.* **2017**, *155*, 154–163. [\[CrossRef\]](#)
55. Morin, V.; Termkhajornkit, P.; Huet, B.; Pham, G. Impact of quantity of anhydrite, water to binder ratio, fineness on kinetics and phase assemblage of belite-ye’elimite-ferrite cement. *Cem. Concr. Res.* **2017**, *99*, 8–17. [\[CrossRef\]](#)
56. Jeong, Y.; Hargis, C.W.; Chun, S.C.; Moon, J. The effect of water and gypsum content on strätlingite formation in calcium sulfoaluminate-belite cement pastes. *Constr. Build. Mater.* **2018**, *166*, 712–722. [\[CrossRef\]](#)
57. Chen, I.A.; Juenger, M.C.G. Synthesis and hydration of calcium sulfoaluminate-belite cements with varied phase compositions. *J. Mater. Sci.* **2011**, *46*, 2568–2577. [\[CrossRef\]](#)
58. Zhang, L.; Glasser, F.P. Hydration of calcium sulfoaluminate cement at less than 24 h. *Adv. Cem. Res.* **2002**, *14*, 15. [\[CrossRef\]](#)
59. Scrivener, K.; Snellings, R.; Lothenbach, B. *A Practical Guide to Microstructural Analysis of Cementitious Materials*; CRC Press: Boca Raton, FL, USA, 2016; ISBN 9781138747234.
60. Rungchet, A.; Poon, C.S.; Chindaprasirt, P.; Pimraksa, K. Synthesis of low-temperature calcium sulfoaluminate-belite cements from industrial wastes and their hydration: Comparative studies between lignite fly ash and bottom ash. *Cem. Concr. Compos.* **2017**, *83*, 10–19. [\[CrossRef\]](#)
61. Shen, Y.; Li, X.; Chen, X.; Zhang, W.; Yang, D. Synthesis and calorimetric study of hydration behavior of sulfate-rich belite sulfoaluminate cements with different phase compositions. *J. Therm. Anal. Calorim.* **2018**, *133*, 1281–1289. [\[CrossRef\]](#)
62. Borštnar, M.; Daneu, N.; Dolenc, S. Phase development and hydration kinetics of belite-calcium sulfoaluminate cements at different curing temperatures. *Ceram. Int.* **2020**, *46*, 29421–29428. [\[CrossRef\]](#)